Clay Minerals (2019), **54**, 153–159
doi:10.1180/clm.2019.22

CAMBRIDGE UNIVERSITY PRESS

Article

Defect and temperature effects on the mechanical properties of kaolinite: a molecular dynamics study

H. Yang, Z.F. Han, J. Hu and M.C. He*

State Key Laboratory for Geomechanics and Deep Underground Engineering, China University of Mining and Technology (Beijing), Beijing 100083, China

Abstract

Molecular dynamics simulations of different defective kaolinites under tension were performed to reveal the effects of defect location, type, density and temperature on their mechanical properties. Four types of defective kaolinite with Si vacancies were constructed. Based on the atomic-scale deformation and failure processes of defective kaolinite and its stress–strain curves, the Young's moduli and tensile strengths in three crystal directions were obtained and compared with the existing theoretical values from the literature. The defect location at each layer does not affect the mechanical properties of kaolinite and the cracks initiated at the defective sites. The atom density of each model was calculated in order to investigate the defect-type effect on the mechanical properties of kaolinite. The simulation results also showed that kaolinite exhibits brittle failure behaviour and the mechanical properties degrade significantly with increasing defect density and temperature. The influence of temperature on the mechanical properties of defective kaolinite is discussed in detail.

Keywords: defect, kaolinite, mechanical properties, molecular dynamics, temperature effect

(Received 4 April 2018; revised 15 January 2019; Accepted Manuscript online: 24 May 2019; Associate Editor: Lawrence Warr)

Clay minerals are layered aluminosilicates occurring in sediments, soils and soft rocks. Clays have various uses and applications in pottery, construction and the mining industry (Murray, 2000). They have also been used in new technological fields over recent decades. For example, clay minerals are used as fillers in polymer nanocomposites (Chen *et al.*, 2008). These materials have excellent properties, such as high dimensional stability, reduced gas permeability and enhanced mechanical properties (Podsiadlo *et al.*, 2007; Ham *et al.*, 2013; Abdi-Khangah *et al.*, 2018). Moreover, various molecules may be intercalated between clay layers, enlarging the volume of the clays and improving their traditional applications (Kakegawa & Ogawa, 2002; Rutkai *et al.*, 2009). Recently, they have also been used as natural or artificial barriers in radioactive waste depositories due to their low permeability and long-term healing capacity (Mondol *et al.*, 2007; Wersin *et al.*, 2007). Although these materials have numerous applications, little work has been carried out on their mechanical properties. This is mainly due to the fact that the small grain size makes it difficult to isolate an individual clay crystallite large enough to satisfy experimental requirements. In addition, their high affinity for water and fine-grained polycrystalline nature make it challenging to measure their physical and chemical properties. Therefore, to fully understand the complex structure of these materials and the critical mechanisms of intercalation, it has become necessary to use modern molecular simulation methods, especially because many of the layered materials are restricted to nano-sized morphologies and are less suitable for conventional experimental analysis.

The atoms in pure clay minerals are arranged regularly and mechanically more durable. However, defects are distributed randomly in clay minerals, which lead the physical and chemical properties of clays to exhibit great variability. For example, Nisar *et al.* (2011) performed first-principles calculations for defective kaolinite in order to determine its electronic structure, atomic geometry and defect formation energies. The results implied that the presence of intrinsic defects will change the electronic structure of kaolinite and influence properties such as cation-retention capacity and drug release. He *et al.* (2009) investigated the formation energetics and charge-doping properties of the extrinsic substitutional defects in kaolinite, which excluded the formation possibility of the defects Cu_{Al} and Zn_{Al} in natural kaolinite. Li *et al.* (2015) studied comprehensively the adsorption behaviour of metal ions on defective kaolinite by using molecular dynamics (MD). They indicated that both the amount and stability of adsorption were enhanced by increasing the number of defects and their sizes. The effect of intrinsic defects, such as vacancies in kaolinite, on the mechanical properties of this mineral has, to our knowledge, not been investigated previously.

Molecular dynamics simulation is an effective tool to probe molecular-level structural, physical and mechanical properties, which are rather difficult to explore directly by macroscopic experiments. Density functional theory (DFT) calculations are also a powerful tool to investigate the physical and chemical properties of materials. However, a very limited number of atoms can be built up by using DFT calculations. In contrast, the MD method can simulate millions of atoms and extract deformation and failure details of a system at the atomic scale. Many researchers have used MD methods to investigate the micro-properties of

*E-mail: mchecumtb@163.com

Cite this article: Yang H, Han ZF, Hu J, He MC (2019). Defect and temperature effects on the mechanical properties of kaolinite: a molecular dynamics study. *Clay Minerals* **54**, 153–159. https://doi.org/10.1180/clm.2019.22

Copyright © Mineralogical Society of Great Britain and Ireland 2019

https://doi.org/10.1180/clm.2019.22 Published online by Cambridge University Press

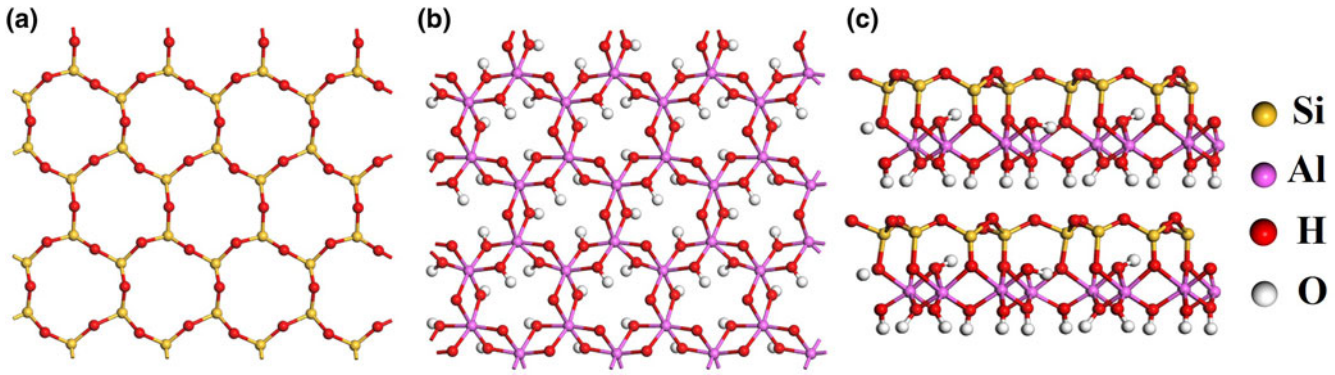


Fig. 1. Structure of kaolinite viewed from (a) Si tetrahedral sheets, (b) Al octahedral sheets and (c) side directions.

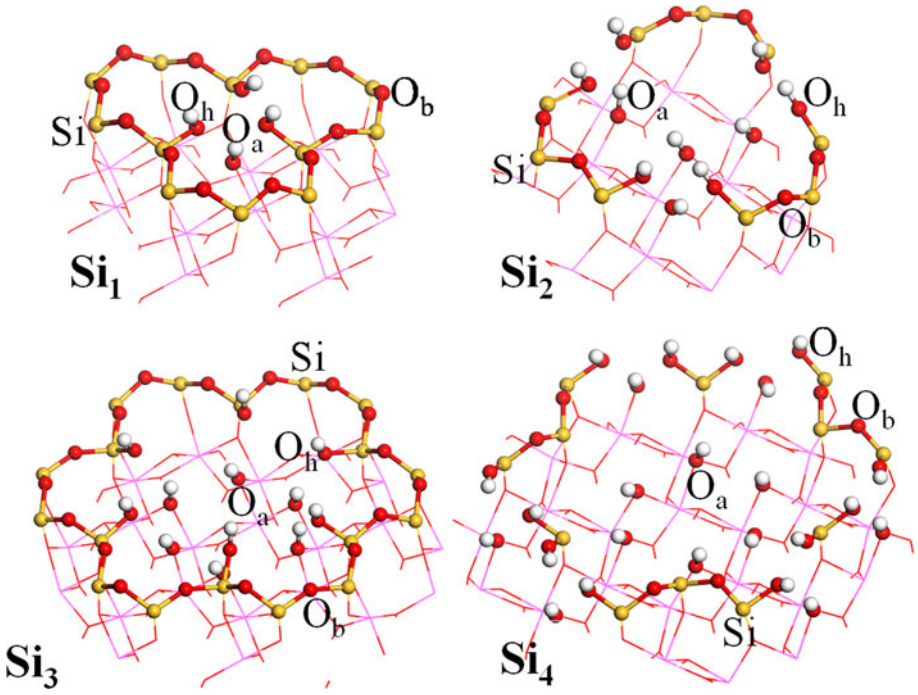


Fig. 2. Enlarged microstructures of various defect types (Si_1, Si_2, Si_3 and Si_4) created at the tetrahedral SiO_4 surface. O_h is from the hydroxyl of silanol and O_a (bridging O) is also bonded to the silanol Si atom, while O_b (bridging O) has no relation to the defect sites.

clay minerals and have obtained satisfactory results (Cygan *et al.*, 2009). For example, Teich-McGoldrick *et al.* (2015) used MD and Monte Carlo simulations to study the effects of layer charge location, interlayer cation and temperature on the swelling of montmorillonite and beidellite clay minerals. Zhang *et al.* (2014) investigated the intercalation behaviour and structure of nanoconfined dodecylamine in kaolinite at the atomic scale. Many studies have also focused on the investigation of the mechanical properties of clay minerals by using MD simulations. For example, Heinz *et al.* (2006) computed cleavage energies for different clay minerals, and these results showed agreement with experimental results. Hantal *et al.* (2014) used the CLAYFF (Cygan *et al.*, 2004) and REAXFF (van Duin *et al.*, 2001) force fields to study the elastic and failure properties of illite at the atomic scale. Teich-McGoldrick *et al.* (2012) used the CLAYFF force field to obtain the mechanical properties of muscovite and observed better agreement with experiment results than earlier DFT calculations. Few of these simulations have involved kaolinite, one of the most abundant clay minerals in the Earth's crust, although Benazzouz and Zaoui (2012) determined the elastic constant tensors of kaolinite under pressure based on MD

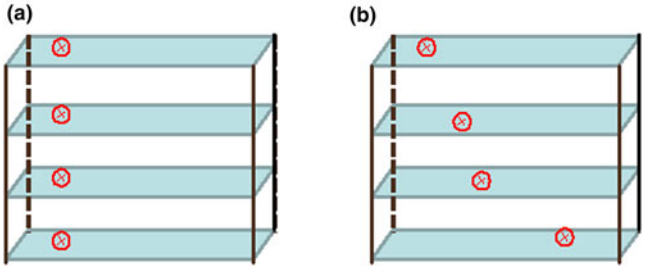


Fig. 3. Schematic diagram of kaolinite with defect locations of (a) type I, and (b) type II. The crosses within circles represent defect sites.

methods. However, there is still a lack of comprehensive research on the microstructural details of kaolinite under deformation. A fundamental question is whether or not the defects would lead to changes in the mechanical properties of kaolinite.

In this study, the effects of defects and temperature on the mechanical properties of kaolinite were studied using classical MD simulations. Kaolinites with four types of

https://doi.org/10.1180/clm.2019.22 Published online by Cambridge University Press

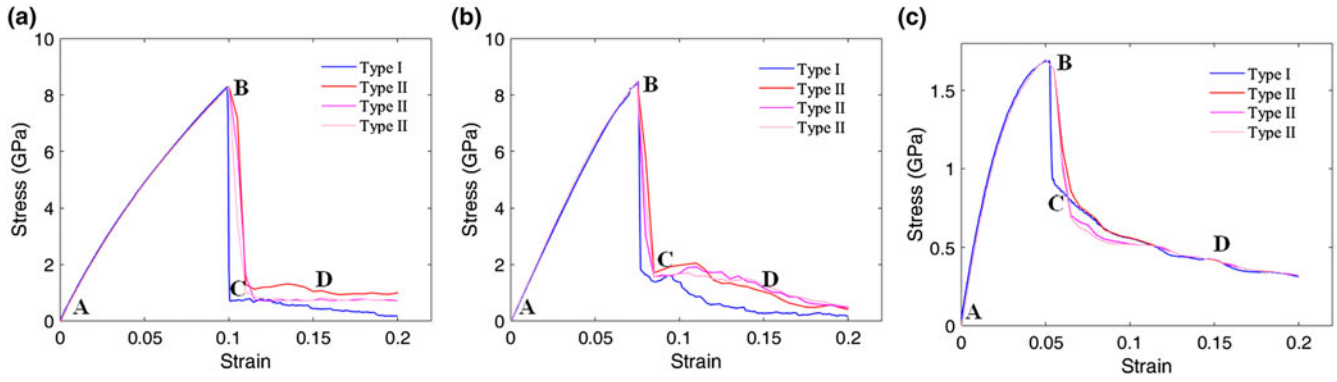


Fig. 4. Stress–strain curves of Si_1 kaolinite along the (a) *OA*, (b) *OB* and (c) *OC* directions.

defect were constructed. The uniaxial tensile stress–strain responses of different defect types, locations and densities were obtained. In addition, the basic mechanical properties, such as Young's modulus and maximum stress, for different defect densities were derived and are discussed in detail. Finally, the temperature effects of kaolinites with different defect types were investigated.

Simulation details

Crystal structures

Kaolinite is a 1:1 clay mineral that is abundant in the Earth's crust. The kaolinite structure consists of a siloxane tetrahedral sheet and a gibbsite-type octahedral sheet (Fig. 1). In the Si tetrahedral sheet (Fig. 1a), each Si atom is connected to three other Si atoms by sharing oxygen atoms, forming the siloxane surface. This arrangement creates hexagonal cavities on the surface. In the Al octahedral sheet (Fig. 1b), each Al atom is coordinated by two vertex oxygen atoms of the siloxane surface and shares four hydroxyls with neighbouring Al atoms. These two sheets are bonded through hydrogen bonds (Fig. 1c).

Defects in kaolinite and montmorillonite have been investigated experimentally, and different types of defect have been observed to be associated with silanol nests (Yamagishi *et al.*, 1991; Fickel *et al.*, 2010; Bayahia *et al.*, 2013). Silanol defects have also been detected in other clay minerals (Libowitzky & Beran, 1995; Khraisheh *et al.*, 2005; Bobon *et al.*, 2011), and it has been proposed that a significant fraction of carbon resources reside in the defects of minerals in the Earth's mantle. Here, MD simulations are employed to simulate the mechanical properties of kaolinite with different silanol defects (Fig. 2). The defect sizes follow the order $Si_1 < Si_2 < Si_3 < Si_4$, with removal of 1, 4, 6 and 10 lattice Si atoms, respectively. The dangling O atoms of defect sites were saturated with H atoms to ensure electroneutrality. In this study, models with 512 unit cells ($16 \times 8 \times 8$ along *OA*, *OB* and *OC* directions) were built and then different defect types were created on the kaolinite models by deleting Si atoms and saturating with O atoms.

Method

Selecting an appropriate interatomic potential is a key task in MD simulations for describing accurately the interactions between atoms. The CLAYFF force field (Cygan *et al.*, 2004) is highly efficient at modelling the crystal structures of kaolinite and montmorillonite (Larentzos *et al.*, 2007; Cygan *et al.*, 2012). In this study, the CLAYFF force field was used to investigate the mechanical behaviour of kaolinite with defects.

The total potential energy includes contributions from Coulombic interactions, van der Waals interactions and any bonded interactions:

$$E_{\text{total}} = E_{\text{Coul}} + E_{\text{VDW}} + E_{\text{bond-strech}}$$
$$= \frac{e^2}{4\pi\varepsilon_0}\sum_{i\neq j}\frac{q_i q_j}{r_{ij}} + \sum_{i\neq j} D_{0,ij}\left[\left(\frac{R_{0,ij}}{r_{ij}}\right)^{12} - 2\left(\frac{R_{0,ij}}{r_{ij}}\right)^{6}\right] + k_1(r_{ij}-r_0)^2 \quad (1)$$

where r_{ij} is the distance between atoms i and j. The first term is Coulombic energy, where e is the charge of an electron, ε_0 is the dielectric permittivity of a vacuum (8.85419×10^{-12} F/m) and q_i and q_j are the atomic partial charges, which can be derived from quantum mechanics calculations. The second term is van der Waals energy, $D_{0,ij}$ and $R_{0,ij}$, which can be derived as:

$$R_{0,ij} = \frac{1}{2}(R_{0,i} + R_{0,j}) \quad (2)$$

$$D_{0.ij} = \sqrt{D_{0,i}D_{0,j}} \quad (3)$$

The third term represents the bonded stretch energy (O–H), where $k_1 = 554.1349$ kcal/mol Å^2 is a force constant and $r_0 = 1$ Å is the equilibrium bond length. The force field parameters of saturated O_a–H pairs are the same as the hydroxyl groups (O–H) in the CLAYFF force field.

All of the simulations were performed using open-source parallel code *LAMMPS* (Plimpton, 1995). The *OA*, *OB* and *OC* coordination axes correspond to the crystallographic orientations [1 0 0], [0 1 0] and [0 0 1], respectively. The periodic boundary condition is used for all directions to remove possible surface effects. The NVT (with a constant particle number–volume–temperature at 300 K) and NPT (with a constant particle number–pressure–temperature at 300 K and 1.0 atmosphere) ensembles were implemented here with a Nosé–Hoover thermostat and barostat.

The mechanical properties of regular and defective kaolinite were investigated using MD simulations. First, the regular kaolinite was built by reduplicating the unit cell in *OA*, *OB* and *OC*

https://doi.org/10.1180/clm.2019.22 Published online by Cambridge University Press

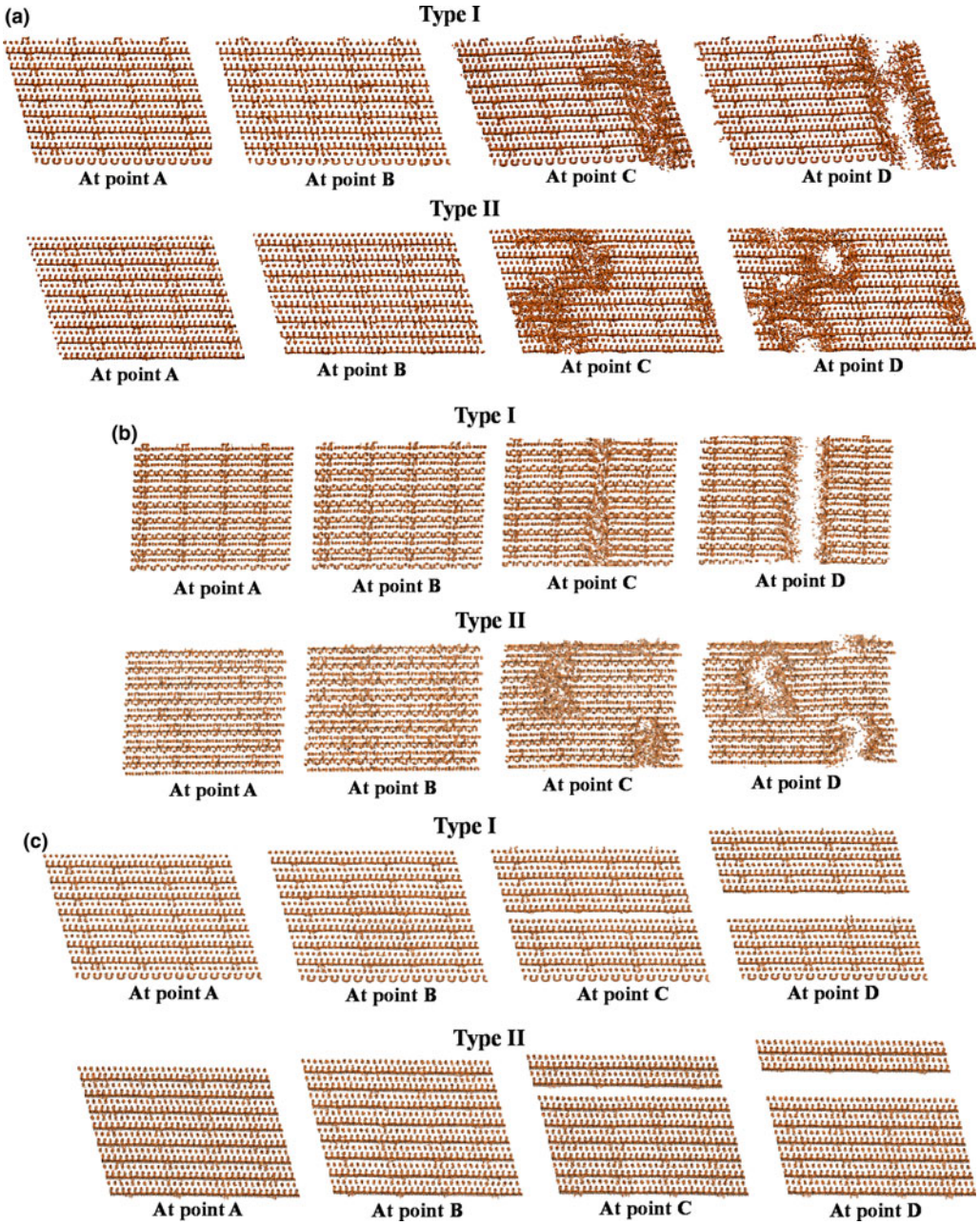


Fig. 5. The corresponding microstructures of kaolinite with type I and II defect locations at four specific points in the (a) *OA*, (b) *OB* and (c) *OC* directions.

directions. Then, defective kaolinite models with different defect densities were generated by removing Si atoms in the SiO_4 surface based on the regular kaolinite model. Finally, tensile tests were carried out by continuously increasing deformation along their corresponding axes; three uniaxial tension tests were performed on an equilibration configuration. The stress was determined by summing up the internal forces at individual particle points and dividing by the initial system area. To obtain a freestanding configuration, a given system was relaxed for 50 ps through NVT (with a constant particle number–volume–temperature at 300 K) and NPT (with a constant particle number–pressure–temperature at 300 K and 1.0 atmosphere) ensembles sequentially, and it reached an equilibrium state. Previous studies (Rottler & Robbins, 2003; Lyulin *et al.*, 2006; Mahajan & Basu, 2010) have indicated that MD is a useful tool for investigating qualitatively the relationship between micro-scale phenomena and macro-scale mechanical properties and, to some extent, to determine quantitatively these terms. However, there is significant discrepancy between the simulated and experimental strain rates. Due to the computational costs and the time required to produce results that are qualitatively similar to experimental results, MD simulations typically use strain rates that are about six to ten orders of magnitude larger than the highest strain rates commonly used in experiments (Sahputra & Echtermeyer, 2013). We tested the effect of strain rate on mechanical behaviour using three different strain rates (5×10^8, 5×10^9 and 5×10^{10} s^{-1}). Negligible change was observed in the results as a function of strain rate (Fig. S1 in Supplementary Information). In order to save computational time and to obtain sufficient configurations under different strains, one cell direction was continuously

https://doi.org/10.1180/clm.2019.22 Published online by Cambridge University Press

Table 1. Young's moduli and maximum stresses of kaolinite with different defect densities in the *OA*, *OB*, and *OC* directions.

Direction		Young's modulus (GPa)			Maximum stress (GPa)		
		OA	*OB*	*OC*	*OA*	*OB*	*OC*
Defect density	0	92 ± 3.2	170 ± 5.1	31 ± 1.4	10.02 ± 0.4	11.87 ± 0.4	1.73 ± 0.3
	0.125	90 ± 3.0	122 ± 4.2	30 ± 1.5	9.26 ± 0.4	8.45 ± 0.3	1.70 ± 0.2
	0.250	84 ± 2.5	108 ± 3.7	30 ± 1.5	8.30 ± 0.3	8.20 ± 0.2	1.69 ± 0.3
	0.500	77 ± 2.2	97 ± 3.4	29 ± 1.6	7.93 ± 0.3	6.51 ± 0.3	1.63 ± 0.3

deformed by a strain rate of 5×10^9 s^{-1}. The timestep is set to be 1.0 fs and the motion of atoms was integrated by using a Verlet leapfrog algorithm.

Results and discussion

Effect of defect location

Kaolinite is a 1:1 layered clay mineral with two types of defect in each layer. In type I, the locations of the defects are the same in each layer, and in type II, the defects are distributed randomly in each layer (Fig. 3). The stress–strain curves of Si_1 kaolinite with different locations of defects are shown in Fig. 4, where point A refers to the initial system without strain and points B, C and D are the strained states at the maximum stress, under inflection and after failure, respectively. Three types of defect location are selected randomly for type II kaolinite. The stress–strain curves of defect location for type II kaolinite are nearly coincident (Fig. 4). In addition, the tensile strength and Young's modulus of kaolinite are almost the same for both defect types, suggesting that the location of defects does not affect the mechanical properties of kaolinite. In addition, the stress increases linearly with increasing strain in the elastic stage before decreasing sharply at the maximum stress, which is due to the fact that the fracture occurred in each layer at the same time. The microstructure change in kaolinite was tracked at different defect locations during tension (Fig. 5). The crack was initiated at the defect sites and propagated very quickly once crack nucleation appeared, which led to the stress drop. Moreover, for the *OA* and *OB* directions, the crack growth trajectory of type I kaolinite is linear since the defect locations are the same in each layer. However, the cracks propagated randomly in each layer for type II kaolinite. The deformation processes of types I and II defective kaolinites are the same when loading along the *OC* direction as only hydrogen bonds between layers are broken.

Effect of defect density

Si_1 defective kaolinite models with different defect densities were built. Here, the defect density is defined as the ratio of the number of defective nests generated to the total number of unit nests in the kaolinite structure. The Young's modulus and tensile strength of regular kaolinite and those of kaolinite with different defect densities of Si vacancies at room temperature are shown in Table 1. The Young's moduli and maximum stress decreased with increasing defect density, which indicates that more vacancy defects degrade the stiffness of materials. Sato *et al.* (2005) calculated the Young's modulus of regular kaolinite at three directions by using DFT calculations, with the corresponding values of Young's moduli in the *OA*, *OB* and *OC* directions being 92, 170 and 31 GPa, respectively, which are in accord with the MD simulation results of this study. Furthermore, in comparison with

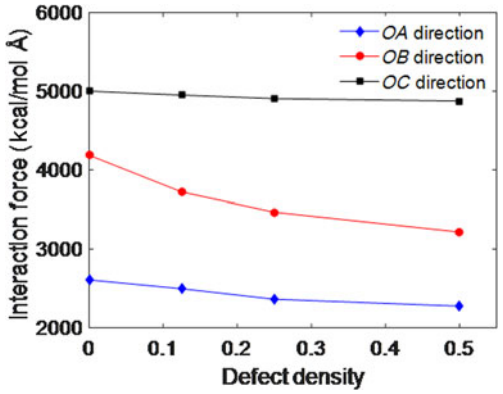


Fig. 6. Interaction force in the *OA*, *OB* and *OC* directions.

Table 2. Atom densities and Young's moduli of kaolinite with different defect types.

Defect type	Atom density (u/Å^3)	Young's modulus (GPa)		
		OA	*OB*	*OC*
Si_0	1.2343	92.00 ± 3.2	170.00 ± 5.1	31.00 ± 1.4
Si_1	1.2247	77.84 ± 2.2	97.31 ± 3.4	29.62 ± 1.6
Si_2	1.1770	50.75 ± 1.8	39.48 ± 1.5	29.26 ± 1.4
Si_3	1.2099	70.23 ± 2.3	92.31 ± 3.3	30.09 ± 1.5
Si_4	1.1861	52.62 ± 2.0	42.59 ± 2.4	29.59 ± 1.3

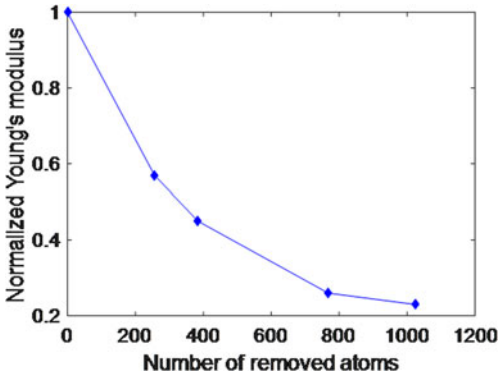


Fig. 7. Normalized Young's moduli of systems with different numbers of removed atoms.

kaolinite without defects, the Young's moduli of defective kaolinite decrease more sharply in the *OB* direction, suggesting that the Si vacancies affect severely the mechanical properties of kaolinite in the *OB* direction. This is because the interaction force decreased most significantly in the *OB* direction (Fig. 6). However, the Young's moduli in the *OC* direction hardly changed with the variation of defect density, because the OH···O hydrogen bonds, which are the dominant interactions between layers and Si vacancies, have little effect in the *OC* direction.

Effect of defect type

The atom density of defective kaolinite is defined as:

$$\rho = \frac{m}{V} \tag{4}$$

https://doi.org/10.1180/clm.2019.22 Published online by Cambridge University Press

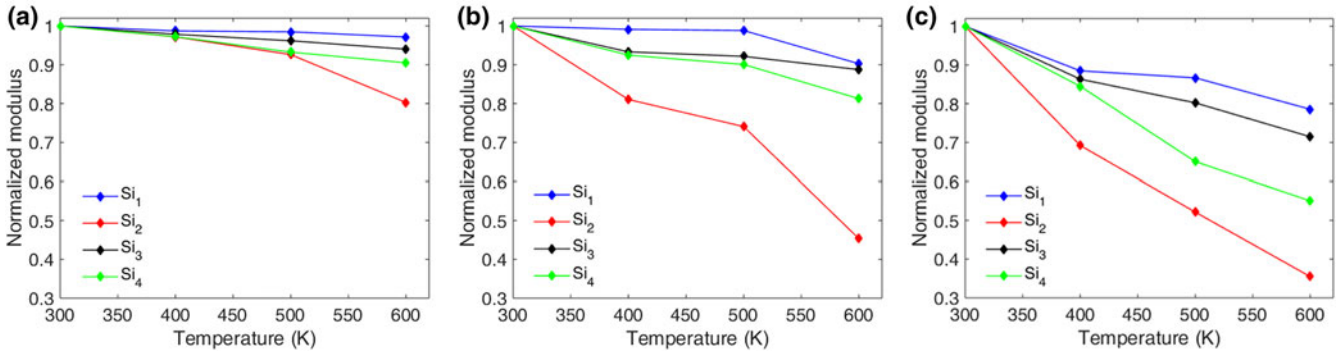


Fig. 8. Normalized Young's moduli of kaolinite at different temperatures in the (a) *OA*, (b) *OB* and (c) *OC* directions.

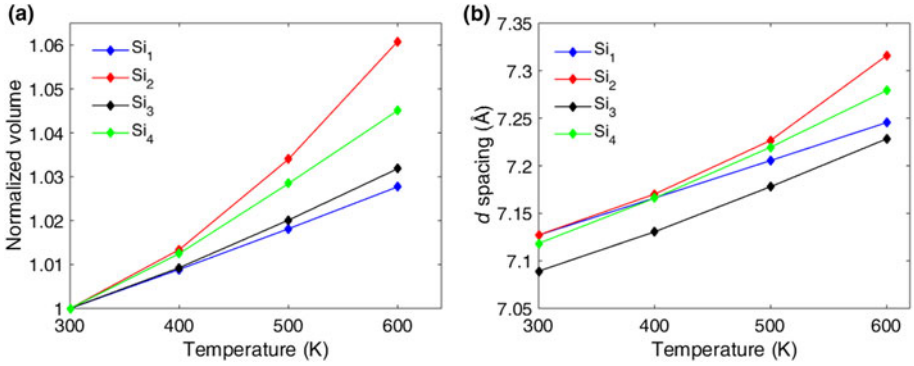


Fig. 9. (a) Normalized volumes and (b) *d* spacings of kaolinite at different temperatures.

where *m* is the mass of atoms and *V* is the volume of the system. The defect density of 50% was selected to investigate the effect of the defect type of kaolinite. The numbers of Si atoms removed in Si_1, Si_2, Si_3 and Si_4 systems are 256, 1024, 384 and 768, respectively. The atom density and Young's modulus of kaolinite with different defect types in the *OA* and *OB* directions both follow the order $Si_2 < Si_4 < Si_3 < Si_1 < Si_0$ (Table 2). Here, Si_0 represented the system with no defects. The normalized Young's moduli are shown in Fig. 7 with increasing numbers of removed atoms. Here, the moduli were normalized by using the Young's modulus of the Si_0 system. The results indicate that the more atoms that were removed, the weaker the mechanical properties of kaolinite. This is because removing more Si atoms leads to lower atom density, which weakens interactions between atoms and decreases the Young's modulus and strength of kaolinite.

Effect of temperature

Four temperatures (300, 400, 500 and 600 K) and a defect density of 50% were selected to investigate the temperature effect of kaolinite with different types of defect. The normalized Young's moduli in the *OA*, *OB* and *OC* directions are shown in Fig. 8. Here, the normalized moduli of the three directions were calculated by using their respective values at 300 K. The moduli decrease with increasing temperature in all of the directions. This is due to the fact that the volume of kaolinite expanded with increasing temperature, which weakened the interactions between atoms (Fig. 9a). Moreover, the greater the volume expansion, the faster the modulus decrease, and thus the temperature sensitivity of defective kaolinite follows the order $Si_2 > Si_4 > Si_3 > Si_1$, which has the same trend as that for atom density. In addition, the modulus in the *OC* direction decreased the most. As is shown in Table 2, Si vacancies affected most significantly the mechanical properties in the *OA* and *OB* directions. The *OC* direction is dominated by hydrogen bonds, which indicate that basal *d* spacing is more sensitive to temperature compared with the Si defects.

Conclusions

The mechanical properties of kaolinite with Si vacancies were investigated using MD simulations. Uniaxial tension tests of defective kaolinite models under various conditions, including defect type, location and density effects, were carried out, and the stress–strain curves in three crystal directions were obtained. The stress–strain relationships of kaolinite with different defect locations in each layer are almost the same, and the defect sites are the weakest points, thereby initiating and propagating the cracks. The Young's modulus and maximum stress exhibit significant decreases as defect density or temperature increase. The decrease with temperature seen in the mechanical properties might be attributed to the thermal expansion of defective kaolinite in the *OA*, *OB* and *OC* directions. The results obtained will be helpful in understanding related defective minerals.

Supplementary material. To view supplementary material for this article, please visit https://doi.org/10.1180/clm.2019.22

Acknowledgements. This work was supported by the National Key Research and Development Program (2016YFC0600901) and the Chinese Postdoctoral Foundation (2017M611043).

References

Abdi-Khangah M., Barati H. & Zhang Z. (2018) Stability analysis of xanthan–Cr(III)–clay nanocomposite gel: an experimental investigation. *Energy & Fuels*, **32**, 2640–2640.

Bayahia H., Kozhevnikova E. & Kozhevnikov I. (2013) High catalytic activity of silicalite in gas-phase ketonisation of propionic acid. *Chemical Communications*, **49**, 3842–3844.

Benazzouz B.K. & Zaoui A. (2012) A nanoscale simulation study of the elastic behaviour in kaolinite clay under pressure. *Materials Chemistry and Physics*, **132**, 880–888.

Bobon M., Christy A.A., Kluvanec D. & Illasova L.U. (2011) State of water molecules and silanol groups in opal minerals: a near infrared spectroscopic study of opals from Slovakia. *Physics and Chemistry of Minerals*, **38**, 809–818.

Chen B., Evans J.R., Greenwell H.C., Boulet P., Coveney P.V., Bowden A.A. & Whiting A. (2008) A critical appraisal of polymer–clay nanocomposites. *Chemical Society Reviews*, **37**, 568–594.

Cygan R.T., Greathouse J.A., Heinz H. & Kalinichev A.G. (2009) Molecular models and simulations of layered materials. *Journal of Materials Chemistry*, **19**, 2470–2481.

Cygan R.T., Liang J.J. & Kalinichev A.G. (2004) Molecular models of hydroxide, oxyhydroxide, and clay phases and the development of a general force field. *Journal of Physical Chemistry B*, **108**, 1255–1266.

Cygan R.T., Romanov V.N. & Myshakin E.M. (2012) Molecular simulation of carbon dioxide capture by montmorillonite using an accurate and flexible force field. *Journal of Physical Chemistry C*, **116**, 13079–13091.

Fickel D.W., Shough A.M., Doren D.J. & Lobo R.F. (2010) High-temperature dehydrogenation of defective silicalites. *Microporous and Mesoporous Materials*, **129**, 156–163.

Ham M., Kim J.C. & Chang J.H. (2013) Thermal property, morphology, optical transparency, and gas permeability of PVA/SPT nanocomposite films and equi-biaxial stretching films. *Polymer Korea*, **37**, 579–586.

Hantal G., Brochard L., Laubie H., Ebrahimi D., Pellenq R.J.M., Ulm F.J. & Coasne B. (2014) Atomic-scale modelling of elastic and failure properties of clays. *Molecular Physics*, **112**, 1294–1305.

He M.C., Fang Z.J. & Zhang P. (2009) Theoretical studies on defects of kaolinite in clays. *Chinese Physics Letters*, **5**, 262–265.

Heinz H., Vaia R.A. & Farmer B.L. (2006) Interaction energy and surface reconstruction between sheets of layered silicates. Journal of Chemical Physics, *124*, 224713.

Kakegawa N. & Ogawa M. (2002) The intercalation of beta-carotene into the organophilic interlayer space of dialkyldimethylammonium-montmorillonites. *Applied Clay Science*, **22**, 137–144.

Khraisheh M.A.M., Al-Ghouti M.A., Allen S.J. & Ahmad M.N. (2005) Effect of OH and silanol groups in the removal of dyes from aqueous solution using diatomite. *Water Research*, **39**, 922–932.

Larentzos J.P., Greathouse J.A. & Cygan R.T. (2007) An *ab initio* and classical molecular dynamics investigation of the structural and vibrational properties of talc and pyrophyllite. *Journal of Physical Chemistry C*, **111**, 12752–12759.

Li X., Li H. & Yang G. (2015) Promoting the adsorption of metal ions on kaolinite by defect sites: a molecular dynamics study. *Scientific Reports*, **5**, 14377.

Libowitzky E. & Beran A. (1995). OH defects in forsterite. *Physics and Chemistry of Minerals*, **22**, 387–392.

Lyulin A.V., Li J., Mulder T., Vorselaars B. & Michel M.A.J. (2006) Atomistic simulation of bulk mechanics and local dynamics of amorphous polymers. *Macromolecular Symposia*, **237**, 108–118.

Mahajan D.K. & Basu S. (2010) On the simulation of uniaxial, compressive behaviour of amorphous, glassy polymers with molecular dynamics. *International Journal of Applied Mechanics*, **2**, 515–541.

Mondol N.H., Bjorlykke K., Jahren J. & Hoeg K. (2007) Experimental mechanical compaction of clay mineral aggregates – changes in physical properties of mudstones during burial. *Marine and Petroleum Geology*, **24**, 289–311.

Murray H.H. (2000) Traditional and new applications for kaolin, smectite, and palygorskite: a general overview. *Applied Clay Science*, **17**, 207–221.

Nisar J., Århammar C., Jämstorp E. & Ahuja R. (2011) Optical gap and native point defects in kaolinite studied by the GGA-PBE, HSE functional, and GW approaches. *Physical Review B*, **84**, 2250–2262.

Plimpton S. (1995) Fast parallel algorithms for short-range molecular dynamics. *Journal of Computational Physics*, **117**, 1–19.

Podsiadlo P., Kaushik A.K., Arruda E.M., Waas A.M., Shim B.S., Xu J. & Ramamoorthy A. (2007) Ultrastrong and stiff layered polymer nanocomposites. *Science*, **318**, 80–83.

Rottler J. & Robbins M.O. (2003) Shear yielding of amorphous glassy solids: effect of temperature and strain rate. Physical Review E, *68*, 011507.

Rutkai G., Mako E. & Kristof T. (2009) Simulation and experimental study of intercalation of urea in kaolinite. *Journal of Colloid and Interface Science*, **334**, 65–69.

Sahputra I.H. & Echtermeyer A.T. (2013) Effects of temperature and strain rate on the deformation of amorphous polyethylene: a comparison between molecular dynamics simulations and experimental results. *Modelling and Simulation in Materials Science and Engineering*, **21**, 065016.

Sato H., Ono K., Johnston C.T. & Yamagishi A. (2005) First-principles studies on the elastic constants of a 1:1 layered kaolinite mineral. *American Mineralogist*, **90**, 1824–1826.

Teich-McGoldrick S.L., Greathouse J.A. & Cygan R.T. (2012) Molecular dynamics simulations of structural and mechanical properties of muscovite: Pressure and temperature effects. *Journal of Physical Chemistry C*, **116**, 22–45.

Teich-McGoldrick S.L., Greathouse J.A., Jovécolón C.F. & Cygan R.T. (2015) Swelling properties of montmorillonite and beidellite clay minerals from molecular simulation: comparison of temperature, interlayer cation, and charge location effects. *Journal of Physical Chemistry C*, **119**, 20880–20891.

van Duin A.C.T., Dasgupta S., Lorant F. & Goddard W.A. (2001) ReaxFF: a reactive force field for hydrocarbons. *Journal of Physical Chemistry A*, **105**, 9396–9409.

Wersin P., Johnson L.H. & McKinley I.G. (2007) Performance of the bentonite barrier at temperatures beyond 100 degrees C: a critical review. *Physics and Chemistry of the Earth*, **32**, 780–788.

Yamagishi K., Namba S. & Yashima T. (1991) Defect sites in highly siliceous HZSM-5 zeolites: a study performed by alumination and IR spectroscopy. *Journal of Physical Chemistry*, **95**, 872–877.

Zhang S., Liu Q., Cheng H., Li X., Zeng F. & Frost R.L. (2014) Intercalation of dodecylamine into kaolinite and its layering structure investigated by molecular dynamics simulation. *Journal of Colloid & Interface Science*, **430**, 345–350.

https://doi.org/10.1180/clm.2019.22 Published online by Cambridge University Press